



A01-16109

**AIAA 2001-0194**

**LES of Combustion Dynamics in a  
Pulse Combustor**

K. Tajiri and S. Menon  
*School of Aerospace Engineering  
Georgia Institute of Technology  
Atlanta, Georgia 30332-0150*

**39th AIAA Aerospace Sciences Meeting &  
Exhibit**

**January 8-11, 2001 / Reno, NV**

# LES of Combustion Dynamics in a Pulse Combustor

K. Tajiri\* and S. Menon†  
*School of Aerospace Engineering  
Georgia Institute of Technology  
Atlanta, Georgia 30332-0150*

Simulation of combustion process in a pulse combustor is carried out to understand the dynamics of flameholding, flow-chemistry interaction and the resulting pulsation. To simulate natural pulsation, a characteristic based boundary condition was modified to simulate the behavior of the flapper valve. Large-eddy simulations (LES) in an axisymmetric configuration are carried out for a range of combustor dimensions. The inflow boundary conditions automatically synchronizes with the acoustic mode and results in steady-state pulsation in this device. Results show that strain-induced extinction upstream of the flameholder is critical in achieving oscillation at the expected frequency. A scaling analysis is also carried out whereby the pulse combustor dimensions are reduced from typical systems of the order of 1 meter to as small as 15 cm to determine if the dynamics can be reproduced even in such small devices. Potential application of these small pulse combustors for micro-scale heat transfer is also discussed.

## 1 Introduction

The pulse combustor is a simple device consisting of a small combustor attached to a long pipe. Fuel-air mixture enters the combustor from the opposite end of the tail pipe location through an inlet valve. Periodic (pulse) combustion in the combustor is driven/maintained by the acoustic mode in the tail pipe. The concept of the pulse combustor is not new and many such devices are in operation. A key application of this device is in heat transfer since the combustion efficiency of this device is very high.

Two types of pulse combustors have been developed and they differ primarily in the design of their inlet valve. The aerodynamical valve type is designed so that the pressure loss in the direction of the reverse flow in the inlet is higher than the pressure loss in the forward direction. The mechanical-valve type uses either a flapper valve or a rotary valve. The flapper valve, which is very popular, are installed at the inlet to prevent combustion flashback into the inlet and permits a simple control of air and fuel flow rates. On the other hand, this type of combustor has moving parts which can lead to fatigue problem. The rotary valve type requires a feedback system to synchronize the rotation of the valve and the optimum operating frequency of the combustor, and therefore, has not been very popular.

The operation of the pulse combustor occurs in three phases. In the first phase, ignition of the combustible mixture occurs by the remaining hot burned gas from the previous cycle. The burned gas expands and moves

outward towards the inlet and the exit of the combustion chamber. In the second phase the burned gas moves out through the tail pipe and the pressure in the combustion chamber falls. The pressure eventually falls below the atmospheric pressure (or upstream pressure) due to the momentum effect of the outward moving gases and eventually the outflow slows down. In the third phase the combustible fluid-air mixture enter the combustor. The momentum effects cause the pressure to rise above the ambient value. Due to high temperature in the combustor this fresh mixture self-ignites and thus, the entire oscillatory cycle repeats itself.

The primary advantage of the pulse combustor is the enhancement of the momentum, heat, and mass transfer process due to pulsating combustion.<sup>1</sup> For non-premixed combustion, the improved mixing of fuel and air within the combustor reduces the combustor size and the amount of the excess air required to achieve complete combustion. The reduced amount of the excess air decreases the exhaust flow losses, and therefore, increases the thermal efficiency.

Another benefit is the reduction of  $NO_x$  formation. High heat transfer rates to the combustor walls and the rapid and effective mixing of the cooler combustion chamber gases with the hot combustion products result in a short residence time for combustion products at high temperature. This decreases the production of thermal  $NO_x$ .

The physical mechanism by which this system achieves self-sustained oscillation is also well known and is related to the Rayleigh criterion. In order to achieve pulsating combustion, heat release spontaneously excites pressure (acoustic) oscillation and when the periodic heat release is in-phase with the nat-

\*Graduate Research Assistant, AIAA Student Member

†Professor, Associate Fellow

Copyright © 2001 by K. Tajiri and S. Menon. Published by the American Institute of Aeronautics and Astronautics, Inc. with permission.

ural acoustic mode of the tail pipe then energy is added to the acoustic mode and the system begins to resonate at the natural mode of the tail pipe. Typically, the pulsation occurs at the tail pipe's quarter-wave acoustic mode frequency.

Although many experimental studies have been carried out for the pulse combustor only a few numerical studies have been reported in the literature. Furthermore, all reported studies employed simplifications or ad hoc boundary conditions in order to create and sustain the pulsations. For example, Tsujimoto *et al.*<sup>2</sup> analyzed the Helmholtz-type pulse combustor numerically using the method of characteristics. First, they examined a simple acoustic model to show that a phase lag in the combustion plays an important role in pulse combustion. Then they assumed that combustion started at a certain time after the introduction of fresh air and fuel and showed that a constant combustion delay time model could simulate most of the important features observed in the pulse combustor.

Barr *et al.*<sup>3</sup> developed a one-dimensional numerical model of a pulse combustor. The unsteady, one-dimensional equations of continuity, momentum, and energy were solved using MacCormack method with variable-area geometry, including losses due to friction and heat transfer. The periodic injection of mass into the combustion chamber was handled by switching between solid and open boundary conditions. To simulate the periodic influx of reactants and to excite the oscillation, the inflow was explicitly forced at the expected natural mode of the inlet pipe. Since the mass flow was forced, a fixed mass influx was forced into the combustion chamber when the valve was open. For the modeling of the combustion and heat release, they distributed the heat uniformly within the combustion chamber.

In later studies, Barr *et al.*<sup>4,5</sup> investigated the effect of fuel-air injection, mixing, chemical kinetics and flame extinction. They observed that the operating frequency was not very sensitive to changes in the heat transfer coefficient, while the magnitude of the pulsations could be more sensitive to the heat transfer. Their study of flame extinction was based on the vortex dynamics method combined with a flame sheet algorithm. They showed that flame extinction plays a dominant role in delaying reaction until later in the cycle.

Benelli *et al.*<sup>6</sup> used a commercial CFD software to model the Helmholtz type pulse combustor with self-sustained acoustic vibrations. Numerical model used an axisymmetric  $k - \epsilon$  turbulence model with the Magnussen-Hjertager turbulent reaction rate closure. The inlet valves, when opened, were considered as orifices with a given cross-section and a characteristic pressure drop curve was used to define a constraint between the velocity and the pressure change across the valves.

Möller *et al.*<sup>7</sup> examined the effects of inlet geometry change using Large Eddy Simulation (LES) in a commercial CFD code. The geometry was changed by altering the position of the stagnation plate near the inlet. The operating characteristics in terms of time-resolved pressure and heat release variations, and time-averaged profiles of the temperature and concentrations of  $O_2$  and  $NO_x$  in the tail pipe were investigated. In this study, the flapper valve was modeled by a prescribed mass inflow of air and fuel using a sinusoidal curve for the first half of the combustor cycle and zero mass flow for the second half of the cycle.

As noted above, in all the previous studies, inflow was explicitly specified. In fact, in all the reported cases, the inlet was forced at the expected pulsation frequency or a condition was enforced on the mass flow to achieve the expected pulsation. Therefore, none of the previous studies were able to properly capture the behavior of the inlet valve and did not excite natural pulse combustion in the device.

The present study addresses this issue and demonstrates a simulation model that incorporates proper physical inflow condition in order to capture the pulsation without requiring ad hoc forcing of the inflow. These simulations employ a LES approach and are used to investigate the dynamics of ignition, flame holding, gas expansion and inflow. A gas-fired, mechanically-valved, Helmholtz-type pulse combustor of a scale that has been experimentally studied is first simulated in order to validate the results and to investigate the dynamics of flow-chemistry interaction. Subsequently, a series of simulations are carried out for different size pulse combustors with tail pipe length ranging from 100 cm to 15 cm. The goal of this parametric study was to determine if the dynamics of pulse combustion remains the same over a wide range of device length and if scaling laws can be devised. It is feasible that very small pulse combustors could find new applications as energy transfer devices for small systems such as micro air vehicles, etc.

## 2 Governing Equations

The governing conservation equations of motion for mass, momentum, energy, and species in a compressible, reacting fluid are:

$$\begin{aligned} \frac{\partial \rho}{\partial t} + \frac{\partial \rho u_i}{\partial x_i} &= 0 \\ \frac{\partial \rho u_i}{\partial t} + \frac{\partial}{\partial x_j} [\rho u_i u_j + p \delta_{ij} - \tau_{ij}] &= 0 \\ \frac{\partial \rho E}{\partial t} + \frac{\partial}{\partial x_i} [(\rho E + p) u_i + q_i - u_j \tau_{ji}] &= 0 \\ \frac{\partial \rho Y_m}{\partial t} + \frac{\partial}{\partial x_i} [\rho Y_m (u_i + V_{i,m})] &= \dot{w}_m \quad m = 1, N \end{aligned} \quad (1)$$

Here,  $\rho$  is the mass density,  $p$  is the pressure,  $E$  is the total energy per unit mass,  $u_i$  is the velocity vector,  $q_i$  is the heat flux vector,  $\tau_{ij}$  is the viscous stress tensor, and  $N$  is the total number of chemical species. The individual species mass fraction, diffusion velocities, and mass reaction rate per unit volume are, respectively,

$Y_m$ ,  $V_{i,m}$ , and  $\dot{w}_m$ . The viscous stress tensor is  $\tau_{ij} = \mu(\partial u_i/\partial x_j + \partial u_j/\partial x_i) - \frac{2}{3}\mu(\partial u_k/\partial x_k)\delta_{ij}$  where  $\mu$  is the molecular viscosity coefficient approximated using Sutherland's law. The diffusion velocities are approximated by Fick's law:  $V_{i,m} = (-D_m/Y_m)(\partial Y_m/\partial x_i)$ . Here,  $D_m$  is the  $m$ -th species mixture averaged molecular diffusion coefficient. The pressure is determined from the equation of state for a perfect gas mixture

$$P = \rho T \sum_{m=1}^N Y_m R_u / W_m \quad (2)$$

where  $T$  is the temperature,  $R_u$  is the universal gas constant, and  $W_m$  the species molecular weight. The total energy per unit volume is determined from  $\rho E = \rho(e + \frac{1}{2}u_k^2)$  where  $e$  is the internal energy per unit mass given by  $e = \sum_{m=1}^N Y_m h_m - P/\rho$  and  $h_m$  is the species enthalpy. Finally, the caloric equation of state is given by

$$h_m = \Delta h_{f,m}^0 + \int_{T^0}^T c_{p,m}(T) dT \quad (3)$$

where  $\Delta h_{f,m}^0$  is the standard heat of formation at temperature  $T^0$  and  $c_{p,m}$  is the  $m$ -th species specific heat at constant pressure.

Following Erlebacher *et al.*,<sup>8</sup> the flow variables can be decomposed into the supergrid (i.e., resolved) and subgrid (i.e., unresolved) components by a spatial filtering operation such that  $f = \tilde{f} + f''$  where  $\tilde{\phantom{f}}$  and  $f''$  denote resolved supergrid and unresolved fluctuating subgrid quantities, respectively. The LES-resolved supergrid quantities are determined by Favre filtering:

$$\tilde{f} = \frac{\overline{\rho f}}{\bar{\rho}} \quad (4)$$

where the overbar represents spatial filtering defined as

$$\overline{f(x_i, t)} = \int f(x'_i, t) G_f(x_i, x'_i) dx'_i. \quad (5)$$

Here,  $G_f$  is the filter kernel and the integral is over the entire domain. Applying the filtering operation (a low-pass filter of grid size  $\bar{\Delta}$ ) to the Navier-Stokes equations, the following LES equations are obtained:

$$\begin{aligned} \frac{\partial \bar{\rho}}{\partial t} + \frac{\partial \bar{\rho} \tilde{u}_i}{\partial x_i} &= 0 \\ \frac{\partial \bar{\rho} \tilde{u}_i}{\partial t} + \frac{\partial}{\partial x_j} [\bar{\rho} \tilde{u}_i \tilde{u}_j + \bar{p} \delta_{ij} - \bar{\tau}_{ij} + \tau_{ij}^{sgs}] &= 0 \\ \frac{\partial \bar{\rho} \tilde{E}}{\partial t} + \frac{\partial}{\partial x_i} [(\bar{\rho} \tilde{E} + \bar{p}) \tilde{u}_i + \bar{q}_i - \tilde{u}_j \bar{\tau}_{ji} + H_i^{sgs} + \sigma_i^{sgs}] &= 0 \\ \frac{\partial \bar{\rho} \tilde{Y}_m}{\partial t} + \frac{\partial}{\partial x_i} [\bar{\rho} \tilde{Y}_m \tilde{u}_i - \bar{\rho} \tilde{D}_m \frac{\partial \tilde{Y}_m}{\partial x_i} + \Phi_{i,m}^{sgs} + \theta_{i,m}^{sgs}] &= \bar{w}_m \end{aligned} \quad (6)$$

Here,  $\bar{\tau}_{ij}$  and  $\bar{q}_i$  are approximated in terms of the filtered velocity. The unclosed subgrid terms representing respectively, the subgrid stress tensor, subgrid heat flux, unresolved viscous work, species mass flux, diffusive mass flux, and filtered reaction rate are:

$$\tau_{ij}^{sgs} = \bar{\rho} [\tilde{u}_i \tilde{u}_j - \tilde{u}_i \tilde{u}_j]$$

$$\begin{aligned} H_i^{sgs} &= \bar{\rho} [\widetilde{E u}_i - \tilde{E} \tilde{u}_i] + [\overline{\rho u}_i - \bar{\rho} \tilde{u}_i] \\ \sigma_i^{sgs} &= [\overline{u_j \tau_{ij}} - \tilde{u}_j \bar{\tau}_{ij}] \\ \Phi_{i,m}^{sgs} &= \bar{\rho} [\widetilde{u_i Y_m} - \tilde{u}_i \tilde{Y}_m] \\ \theta_{i,m}^{sgs} &= \bar{\rho} [V_{i,m} \widetilde{Y_m} - \tilde{V}_{i,m} \tilde{Y}_m] \\ \bar{w}_m & \end{aligned} \quad (7)$$

The subgrid stress tensor,  $\tau_{ij}^{sgs}$ , and subgrid heat flux  $H_i^{sgs}$ , have been extensively modeled in the past by employing the subgrid kinetic energy equation,  $k^{sgs}$ , and are, therefore, only briefly discussed. The unresolved viscous work,  $\sigma_i^{sgs}$ , and the diffusive mass flux,  $\theta_{i,m}^{sgs}$ , are neglected in this study. Closure of the species mass flux,  $\Phi_{i,m}^{sgs}$ , is carried out in this study using a gradient-diffusion model. Closure of the filtered reaction rate term,  $\bar{w}_m$ , is also discussed below.

## 2.1 Subgrid Closure

In the present approach, the subgrid stress tensor,  $\tau_{ij}^{sgs}$ , is determined by using the local grid size,  $\bar{\Delta}$ , as the characteristic length scale and the subgrid kinetic energy,  $k^{sgs}$ , as the characteristic velocity scale. The subgrid kinetic energy,  $k^{sgs} = \frac{1}{2}[\widetilde{u_k^2} - \tilde{u}_k^2]$  is obtained by solving the following transport equation:<sup>9</sup>

$$\frac{\partial \bar{\rho} k^{sgs}}{\partial t} + \frac{\partial}{\partial x_i} (\bar{\rho} \tilde{u}_i k^{sgs}) = P^{sgs} - D^{sgs} + \frac{\partial}{\partial x_i} \left( \bar{\rho} \frac{\nu_t}{Pr_t} \frac{\partial k^{sgs}}{\partial x_i} \right) \quad (8)$$

where  $Pr_t$  is the turbulent Prandtl number (taken as constant and equal to 0.90 for this study),  $P^{sgs}$  and  $D^{sgs}$  are the production and dissipation of subgrid kinetic energy, respectively. The production term is defined as,  $P^{sgs} = -\tau_{ij}^{sgs} (\partial \tilde{u}_i / \partial x_j)$ , where  $\tau_{ij}^{sgs}$  is the modeled subgrid stress tensor.  $\tau_{ij}^{sgs}$  is modeled as

$$\tau_{ij}^{sgs} = -2\bar{\rho} \nu_t (\tilde{S}_{ij} - \frac{1}{3} \tilde{S}_{kk} \delta_{ij}) + \frac{2}{3} \bar{\rho} k^{sgs} \delta_{ij} \quad (9)$$

with the eddy viscosity,  $\nu_t = C_\nu (k^{sgs})^{1/2} \bar{\Delta}$  where  $\bar{\Delta}$  is the characteristic LES grid size and the resolved rate-of-strain tensor,  $\tilde{S}_{ij} = \frac{1}{2}(\partial \tilde{u}_i / \partial x_j + \partial \tilde{u}_j / \partial x_i)$ .

Finally, the dissipation term is modeled as  $D^{sgs} = C_\epsilon \bar{\rho} (k^{sgs})^{2/3} / \bar{\Delta}$ . The coefficients,  $C_\nu$  and  $C_\epsilon$  can be dynamically determined<sup>10</sup> but will be taken as constants and equal to 0.2 and 0.916, respectively. It should be noted that 3-D isotropic turbulent scaling laws were used to derive the preceding relations, and therefore, may not be completely applicable in this axi-symmetric study.

The closure of the subgrid heat flux,  $H_i^{sgs}$ , is achieved using a conventional gradient-diffusion model:

$$H_i^{sgs} = -\bar{\rho} \frac{\nu_t}{Pr_t} \frac{\partial \tilde{h}}{\partial x_i} \quad (10)$$

where  $\tilde{h}$  is the resolved scale total mixture enthalpy per unit mass,  $\tilde{h} = \Delta h_{f,m}^0 + \int_{T^0}^T c_{p,m}(T) dT + \frac{1}{2} u_k^2$ .

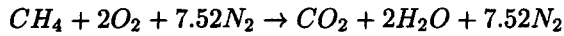
A conventional closure for the subgrid scalar velocity fluctuation term,  $\Phi_{i,m}^{sgs}$ , is a gradient-diffusion model analogous to that used for  $H_i^{sgs}$ :

$$\Phi_{i,m}^{sgs} = -\bar{\rho} \frac{\nu_t}{Sc_t} \frac{\partial \tilde{Y}_m}{\partial x_i} \quad (11)$$

where  $Sc_t$  is the turbulent Schmidt number found from the product,  $Sc_t = Pr_t Le_m$  ( $Le_m$  is the species Lewis number). It should be noted that this form of closure effectively treats small scale fluid dynamic effects as molecular process.

## 2.2 Reaction Rate Closure

A single step, global chemical mechanism for methane/air combustion is currently employed with a molar reaction rate in Arrhenius form.



A pre-exponential term  $A = 3.0 \times 10^8 (\text{sec}^{-1})$  and an activation energy  $E_a = 29,380 (\text{cal/gmol})$  are used. These values are chosen from Smith *et al.*<sup>11</sup>

For LES application, the filtered reaction rate has to be obtained from a closure model. Closure of the fluctuating reaction rate,  $\tilde{w}_m$ , has been accomplished using a modified Eddy-Break-Up (EBU) model based on a model developed earlier. In the EBU model, the time scale required for complete molecular mixing is modeled as the time for one subgrid eddy to be completely dissipated (mixed on the molecular level). Since a subgrid eddy can be viewed as having a uniform composition, the time needed to molecularly diffuse the species is the same that needed for complete velocity dissipation. The subgrid fluid dynamic / mixing time,  $\tau_{mix}$ , is proportional to the subgrid turbulent kinetic energy,  $k^{sgs}$ , and its dissipation rate,  $\epsilon^{sgs}$ , by the relation:

$$\tau_{mix} \sim \frac{k^{sgs}}{\epsilon^{sgs}} \sim C_{EBU} \frac{\bar{\Delta}}{\sqrt{2k^{sgs}}} \quad (12)$$

Here the scaling constant,  $C_{EBU}$ , is set to unity following Fureby *et al.*<sup>12</sup> The mixing time-scale reaction rate for the methane-air premixed lean reaction is, then

$$\dot{w}_{mix} = \frac{1}{\tau_{mix}} [CH_4]. \quad (13)$$

The effective chemical reaction rate,  $\dot{w}_{ebu}$ , is found by taking the minimum of the mixing reaction rate (fluid time scale) and the kinetic rate (chemical time),  $\dot{w}_{kin}$ , i.e.;

$$\dot{w}_{ebu} = \min(\dot{w}_{mix}, \dot{w}_{kin}). \quad (14)$$

## 3 Numerical Method

Axisymmetric, compressible Navier-Stokes equations are solved in the present study using a finite-volume scheme that is second-order-accurate in space

and time. Nearly all practical pulse combustors are axisymmetric in configuration and since the pulsation is primarily driven by the low-frequency longitudinal acoustic mode in the tail pipe, axisymmetric formulation is sufficient to capture all the expected dynamics in the pulse combustor. Some finer details such as the breakdown of the vortices into small-scale eddies (which requires full three-dimensional simulations) are not captured in this approach but they are not considered an important feature for the pulse combustor. Furthermore, from a computational point of view, 3D simulations of the full pulse combustor will require significantly long simulation time (to resolve the long tail pipe and to simulate multiple cyclic pulsations) and therefore, are considered very expensive. Further details of the numerical model and the boundary conditions are given below.

### 3.1 Combustor Geometry

The initial geometry used for validation is nearly identical to the one used in earlier experiments and simulations by Möller *et al.*<sup>7</sup> This pulse combustor is a Helmholtz-type device with a flapper valve. Fuel and air are premixed before they enter the combustion chamber. Although the experimental facility has a rectangular combustion chamber, a cylindrical (axisymmetric) one with the same cross section area is used in this study. In any case, most practical pulse combustors are axisymmetric in cross-section. A schematic of the simulated device is shown in Fig. 1.

The combustion chamber has 45.2mm radius and is 150mm long. It is connected to a tail pipe with an inner radius of 18mm and is 1430mm long. A flame holder (12.5mm radius) is mounted on to a 2.5mm radius rod and is placed on the symmetric axis of the combustor. The inner radius of the inlet tube to the combustion chamber is 10.25mm. Other similar devices were also simulated. Table 1 summarizes the various combustors simulated in the present study.

Relatively high grid resolution has been employed here. The grid resolution is  $190 \times 80$  in the combustion chamber and  $353 \times 48$  in the tail pipe with grid clustering near the walls to resolve the boundary layers. The effect of grid resolution was studied earlier to determine an appropriate resolution in the combustor and in the tail pipe. The grid resolution in the combustor was chosen to resolve the flame structure during the entire period of pulsation while the tail pipe resolution was chosen to resolve the outflow motion and the acoustic mode without requiring significant axial grid stretching. In fact, grid stretching was kept around 5 percent to maintain spatial accuracy of the simulated flow field.

### 3.2 Boundary Conditions

To simulate the behavior of the flapper valve as it is driven by the acoustic oscillation in the tail pipe, "natural" inflow-outflow boundary conditions were de-

combustor	A	B	C
combustion chamber length (m)	0.15	0.045	0.015
combustion chamber radius (m)	0.0452	0.0136	0.0045
inlet area (m <sup>2</sup> )	$3.14 \times 10^{-4}$	$2.82 \times 10^{-5}$	$5.9 \times 10^{-7}$
stagnation plate radius (m)	0.0125	0.00375	0.00125
stagnation plate location (m) (from inlet)	0.013	0.0039	0.0013
tail pipe length (m)	1.43	0.43	0.143
tail pipe radius (m)	0.018	0.0054	0.0018

Table 1 Geometries of various combustors.

veloped. No-slip conditions are prescribed on all the walls, while the symmetric (slip) conditions are prescribed on the symmetric axis. For the thermal wall condition, the combustion chamber walls are treated as adiabatic while a isothermal condition is employed in the tail pipe wall using a linear temperature profile (Fig. 3).<sup>13</sup>

At the inflow, a modified version of the characteristic boundary conditions is imposed. Since the inflow is subsonic, three conditions is prescribed and one condition is computed from inside the computational domain. Here, the stagnation pressure  $p_t$ , the stagnation temperature  $T_t$ , and the angle  $\theta$  of the inflow direction are specified as 101325Pa, 300K and 0°, respectively. Using these quantities other properties such as, pressure, temperature, and radial velocity are obtained as a function of axial flow velocity as follows

$$p = p_t \left[ 1 - \frac{\gamma-1}{\gamma+1} (1 + \tan^2 \theta) \frac{u^2}{a_*^2} \right]^{\frac{\gamma}{\gamma-1}}$$

$$T = T_t \left[ 1 - \frac{\gamma-1}{\gamma+1} (1 + \tan^2 \theta) \frac{u^2}{a_*^2} \right]$$

$$v = u \tan \theta$$

$$a_*^2 = 2\gamma \frac{\gamma-1}{\gamma+1} C_v T_t$$

where  $\gamma$ ,  $C_v$  are specific heat ratio and constant-volume specific heat, respectively. To obtain the axial inflow velocity, a characteristic relation for the upstream moving acoustic wave of the form

$$\frac{\partial p}{\partial t} - \rho c \frac{\partial u}{\partial x} = -(u - c) \left( \frac{\partial p}{\partial x} - \rho c \frac{\partial u}{\partial x} \right)$$

is solved at the inflow. With these boundary conditions, the axial inflow velocity adjusts naturally to the difference between the pressure upstream of the inlet boundary (as determined by the above equations) and the pressure in the combustor just downstream of the inlet. This behavior allows us to simulate the opening and closing of the flapper valve without explicitly controlling the mass inflow. When the interior pressure approaches the upstream (inlet) stagnation pressure, the flow velocity approaches zero and this is used as an indication that the flapper valve is closed. Then,

the boundary conditions of the inlet are changed to a no-slip condition such that the upstream stagnation pressure and the pressure downstream of the inlet are matched and no inflow or reverse flow occurs at the inlet.

At a later stage, when the outflow through the tail pipe occurs and the pressure in the combustor drops below the inlet stagnation pressure, the inflow begins and the cycle repeats itself. Thus, the present inflow condition does not require an explicit specification of the oscillating mass flow and allows the inflow boundary conditions to respond to the pressure oscillation in the combustor. The implications and some surprising consequences of this boundary conditions are discussed later.

For the outflow conditions only the exit pressure is prescribed at the atmospheric condition and characteristic outflow boundary conditions are solved for the three outgoing waves. The four characteristic relations at the exit are

$$\frac{\partial \rho}{\partial t} - \frac{1}{c^2} \frac{\partial p}{\partial t} = -u \left( \frac{\partial \rho}{\partial x} - \frac{1}{c^2} \frac{\partial p}{\partial x} \right)$$

$$\frac{\partial p}{\partial t} + \rho c \frac{\partial u}{\partial t} = -(u + c) \left( \frac{\partial p}{\partial x} + \rho c \frac{\partial u}{\partial x} \right)$$

$$\frac{\partial v}{\partial t} = -u \frac{\partial v}{\partial x}$$

$$\frac{\partial p}{\partial t} - \rho c \frac{\partial u}{\partial t} = -(u - c) \left( \frac{\partial p}{\partial x} - \rho c \frac{\partial u}{\partial x} \right)$$

However, the last condition is replaced the pre-specified pressure condition in the numerical implementation.

### 3.3 Starting Procedure

Although the starting procedure is primarily a numerical artifact, proper initialization and a numerical ignition procedure is required initiate the combustion process and the subsequent pulsations. Here, we tried to follow the procedure used in the experiments to demonstrate the ability of LES method to mimic realistic starting conditions. In the actual pulse combustor it is common to provide a small blower to force a sufficient flow of starting gas. After the pulsation has started the blower and the igniter are turned off.

This procedure is also modeled in the simulations. At the beginning, the combustor is filled with an inert (e.g., burned products) gas. When the simulation starts, the pressure downstream of the tail pipe is reduced to a value slightly below atmospheric (98,000 Pa) and the temperature in the upper combustion chamber wall is set to 2000K to ignite the mixture (Fig. 1). This ignition process is similar to the approach used in the experiments.<sup>14</sup> Due to the pressure difference between the inlet and the exit of the combustor, the fuel-air mixture flows into the combustor and this flow pushes out the initial inert gas. After the combustion chamber is filled up with the fuel-air mixture and the gas starts reacting, the igniter is turned off. Although the first cycle takes longer time to complete compared to the steady operation, the steady state is achieved in 2-3 cycles. Once the combustor starts pulsating, the exit pressure which was reduced for the starting process is raised and reset to the atmospheric value.

For the long tail pipe combustor (combustor A), to achieve sustained oscillation at the expected low frequency of around 100 Hz requires a very long simulation. However, the code is highly optimized for parallel processing and has high scalability. Thus, although a large number of time steps have to be simulated, a typical simulation (of around 5 flow through times after the initial transients) requires around 360 single processor hours on the Cray T3E. Of course, for the small devices the computational cost drops considerably.

## 4 Results and Discussion

In this section, we summarize the results obtained in this study. First, the baseline configuration is simulated to validate the simulation model and then the other sub-scale devices are studied.

Here *cycle time* is defined as follows: the onset of the inflow is 0, the end of the cycle (and the beginning of the next cycle) is 1.0. The fuel-air mixture enters the combustor between cycle time 0 and 0.5, and the flapper valve closes between 0.5 and 1.0.

### 4.1 Self-Sustained Pulsation

To validate the present model, simulations were carried for the test configuration described earlier<sup>7</sup> for which data is available for validation. Fig. 1 shows the schematic of this device and Table 1 summarizes the pertinent dimensions.

The first series of simulations employed the LES model using the EBU closure model for the reaction rate. For these studies no effort was made to take into account the effect of strain-induced extinction observed in the experiments.<sup>15</sup> Fig. 6a-f shows a time sequence of the oscillating filtered reaction rate contours and Fig. 7a-f shows the corresponding temperature contours. As can be seen, during the inflow (Fig. 6b-

d), the hot remnant gases from the previous cycle ignites the fuel-air mixture as it enters the combustor and gets deflected to the upper wall. The flame zone is a narrow band surrounding the reactant mixture. The flame is anchored at two locations: the stagnation plate and the wall along the inlet port. Most of the combustion is completed before the inlet port closes and the flame structure collapses to a region near the inlet. It can be seen that there is still some unburned mixture near the inlet that appears to maintain the flame before the next cycle begins anew. Although this simulation achieved self-sustained steady pulsation the predicted frequency and the mode shape did not agree with experimental observation. This is discussed below.

Fig. 4 shows the pressure oscillation at three locations in the tail pipe. It can be seen that near the combustor exit the pressure oscillation is quite high and reaches around 8 percent peak-to-peak but closer to the exit the pressure amplitude is much lower, less than 2 percent peak-to-peak. Although all locations show a similar frequency, the pressure signature shows a traveling wave.

Analysis of the above pressure signature in terms of mode shape and phase is given in Fig. 5. It can be seen that a three-quarter acoustic mode shape is excited in the tail pipe. The associate frequency is 266 Hz. In contrast, the experimental results reported a quarter-wave mode at a frequency of 103 Hz. Clearly, the simulation discussed above is missing some key physics.

A feature noted in the earlier experiments was that strain-induced extinction occurred in the combustor. However, the above noted simulation ignored this feature. Furthermore, the EBU model described above did not have this feature. The global chemical mechanism does not have any extinction/re-ignition capability and it was considered too expensive to make the chemical kinetic model any more complex for the present study. Furthermore, replacing the EBU model with a more accurate but perhaps more expensive sub-grid combustion model was not considered acceptable for this study.

Therefore, an attempt was made to determine if the EBU model could be modified in a very simplistic manner to mimic local extinction. First, the results of the above noted simulation was analyzed to determine which part of the EBU model, Eqn. 14, was dominating and where. It was determined that during injection and the formation of the initial shear regions (see Fig. 6c-e and Fig. 7c-e) the turbulence mixing time is very small and thus, the EBU model was igniting the mixture using the Arrhenius kinetics. In fact, in most of the near field of the injector combustion was kinetically controlled. If one considers the inverse of the mixing time as a measure of the local strain, it becomes obvious that there are regions in the reacting

zone where strain exceeds  $1000 \text{ sec}^{-1}$ . Clearly, in a real system such a high value of strain should cause local extinction<sup>16</sup> but this feature was not modeled in the above simulation.

Based on this information, another simulation was carried out where an extinction model modification to the EBU was implemented in a very simplistic manner. All regions where the mixing time scale exceeded  $1000 \text{ sec}^{-1}$  was considered extinct and the reaction rate was set to zero. This modification made a drastic change to the oscillation mode and frequency in the combustor.

Figs. 8 and 9 show respectively, the filtered reaction rate and the temperature contours in the combustor with this extinction modification. Significant changes in the combustion process can be observed by comparing these results with the earlier results without extinction (Figs. 6 and 7). Fig. 8 (when compared to Fig. 6) shows that with extinction the reaction zone is no longer a narrow region, rather it is spread out further downstream of the stagnation plate. The flame is still anchored at the plate but since the high strain regions are no longer burning, reactions occur further downstream of the stagnation plate. In the earlier experiments,<sup>15</sup> combustion was seen to occur downstream of the stagnation plate and the present simulation appears to capture this as well.

The impact of the change in the location of burning on the pressure mode is immediately apparent. Figs. 10 and 11 show respectively, the pressure fluctuation and the mode shape for this case. It can be clearly seen that the pressure oscillation is in-phase at all locations in the tail pipe. The peak-to-peak value are not significantly affected by the inclusion of the extinction criteria. The frequency and the mode shape, however, drastically changed from the earlier case. The frequency has reduced to 109 Hz and the mode shape changed from the three-quarter wave to the quarter-wave shape. It is, therefore, clear that the process of combustion and the location of heat release in the combustor can play an important role in determining the oscillation properties.

#### 4.2 Scaling Studies

To determine if the same simulation model is capable of predicting pulsation in much smaller devices, two other combustors (dimensions are given in Table 1) were also simulated using the same model with no changes to the extinction criteria. The dimensions of the devices were scaled down from the reference case to mimic smaller pulse combustors. Both these combustors B and C showed similar steady-state pulsation but at higher frequencies (see Table 2), as was expected. Therefore, only representative results are discussed here.

Fig. 12a shows the mode shape and phase for Combustor B and 12b shows the corresponding results for the combustor C. Clearly, the extinction model and

the inflow/outflow boundary conditions employed in the present study allows simulation of pulse combustion over a wide range of device scales.

There are some qualitative differences in the reaction rate and temperature field for these cases when compared to combustor A. Fig. 13 and 14 shows respectively, the time sequence of the filtered reaction rate and temperature for the combustor C.

In the combustor A there exists high temperature region upstream of the stagnation plate while the combustor C doesn't have such a region. Also high reaction rate and low temperature zone advances far downstream of the plate in the combustor A, whereas the reaction completes near the stagnation plate in the combustor C. One reason of this may be that although the inlet size was decreased the stagnation plate was not changed. This modification can significantly change the combustion dynamics since the turbulent mixing and flame holding can be changed due to geometrical modifications. In fact, it was reported earlier that even a slight change of the inlet geometry can have strong effect on the performance.<sup>7</sup> Nevertheless, the ability of the present simulation model to capture even subtle changes in flow and geometrical parameters provides some confidence that this simulation tool may be useful to study design of pulse combustors even at the small scale.

## 5 Conclusions

Simulation of combustion process in a pulse combustor is carried out to understand the dynamics of flame-holding, flow-chemistry interaction and the resulting pulsation. To simulate natural pulsation, a characteristic based inflow condition was modified to simulate the behavior of the flapper valve. Large-eddy simulations in an axisymmetric configuration are carried out for a range of combustor dimensions. The inflow boundary conditions automatically synchronizes with the acoustic mode and results in steady-state pulsation in this device. Results show that strain-induced extinction upstream of the flameholder is critical in achieving oscillation at the expected frequency. A scaling analysis is also carried out whereby the pulse combustor dimensions are reduced from typical systems of the order of 1 meter to as small as 15 cm to determine if the dynamics can be reproduced even in such small devices. Results suggest that the present model is capable of simulating self-excited pulsation even in very small devices. Although no data is available for such small devices, the predicted frequencies and mode shapes are as expected.

Additional studies are planned to further address the strain-induced extinction effect in more detail. The present study employed a fixed location of the stagnation plate relative to the inlet. Furthermore, the scaling of the size of the stagnation plate was not addressed. By changing the location and the size of

combustor	A	A	A	B	C
	experiment	no extinction model	extinction model	extinction model	extinction model
frequency (Hz)	103	266	109	217	404
mass flow rate (kg/s)	$5.05 \times 10^{-3}$	$6.79 \times 10^{-3}$	$7.55 \times 10^{-3}$	$4.65 \times 10^{-4}$	$7.93 \times 10^{-6}$

**Table 2** Frequencies and mass flow rates for various configuration.

the stagnation plate, the effective mixing process and hence, the mixing time could be modified which in turn would change the local strain rate. Furthermore, since flameholding is a critical issue for self-sustained oscillation, the location and size of the stagnation plate can play a major role. These issues will be addressed in the future. Finally, the ability of the simulation model to capture pulsation in very small devices suggests an opportunity to study even smaller pulse combustors of the order of 1 cm or smaller to determine if this type of device could be used for efficient heat transfer at these scales. Potential applications could be as propulsion or heat transfer devices in micro-air vehicles and other similar small-scale devices.

### References

- <sup>1</sup> Zinn, B. T., "Pulsating Combustion," *Mechanical Engineering*, Vol. 107, No. 8, 1985, pp. 36-41.
- <sup>2</sup> Tsujimoto, Y. and Machii, N., "Numerical Analysis of a Pulse Combustion Burner," *Twenty-first Symposium (International) on Combustion*, 1986, pp. 539-546.
- <sup>3</sup> Barr, P. K., Dwyer, H. A., and Bramlette, T. T., "A One-Dimensional Model of a Pulse Combustor," *Combustion Science and Technology*, Vol. 58, 1988, pp. 315-336.
- <sup>4</sup> Barr, P. K., Keller, J. O., Bramlette, T. T., Westbrook, C. K., and Dec, J. E., "Pulse Combustor Modeling Demonstration of the Importance of Characteristic Times," *Combustion and Flame*, Vol. 82, 1990, pp. 252-269.
- <sup>5</sup> Barr, P. K. and Keller, J. O., "Premixed Combustion in a Periodic Flow Field. Part II: The Importance of Flame Extinction by Fluid Dynamic Strain," *Combustion and Flame*, Vol. 99, 1994, pp. 43-52.
- <sup>6</sup> Benelli, G., De Michele, G., Cossalter, V., Da Lio, M., and Rossi, G., "Simulation of Large Non-Linear Thermo-Acoustic Vibrations in a Pulsating Combustion," *Twenty-fourth Symposium (International) on Combustion*, 1992, pp. 1307-1313.
- <sup>7</sup> Möller, S. I. and Lindholm, A., "Theoretical and Experimental Investigation of the Operating Characteristics of a Helmholtz Type Pulse Combustor due to Changes in the Inlet Geometry," *Combustion Science and Technology*, Vol. 149, 1999, pp. 389-406.
- <sup>8</sup> Erlebacher, G., Hussaini, M. Y., Speziale, C. G., and Zang, T. A., "Toward the Large-Eddy Simulation of Compressible Turbulent Flows," *Journal of Fluid Mechanics*, Vol. 238, 1992, pp. 155-185.
- <sup>9</sup> Menon, S., Yeung, P. K., and Kim, W.-W., "Effect of Subgrid Models on the Computed Interscale Energy Transfer in Isotropic Turbulence," *Computers and Fluids*, Vol. 25, No. 2, 1996, pp. 165-180.
- <sup>10</sup> Kim, W.-W., *A New Dynamic Subgrid-Scale Model for Large-Eddy Simulation of Turbulent Flows*, Ph.D. thesis, Georgia Institute of Technology, Atlanta, GA, September 1996.
- <sup>11</sup> Smith, T. M. and Menon, S., "One-Dimensional Simulations of Freely Propagating Turbulent Premixed Flames," *Combustion Science and Technology*, Vol. 128, 1997, pp. 99-130.
- <sup>12</sup> Fureby, C. and Lofstrom, C., "Large Eddy Simulations of Bluff Body Stabilized Flames," *Twenty-fifth Symposium (International) on Combustion*, 1994, pp. 1257-1264.
- <sup>13</sup> Ku, S. H., *An Investigation of the Gas Fired Pulsating Combustor*, Ph.D. thesis, Georgia Institute of Technology, Atlanta, GA, August 1988.
- <sup>14</sup> Putnam, A. A., Belles, F. E., and Kentfield, J. A. C., "Pulse Combustion," *Progress in Energy and Combustion Science*, Vol. 12, 1986, pp. 43-79.
- <sup>15</sup> Keller, J. O., Barr, P. K., and Gemmen, R. S., "Premixed Combustion in a Periodic Flow Field. Part I: Experimental Investigation," *Combustion and Flame*, Vol. 99, 1994, pp. 29-42.
- <sup>16</sup> Kee, R. J., Miller, J. A., and Evans, G. H., "A Computational Model of the Structure and Extinction of Strained, Opposed Flow, Premixed Methane-Air Flames," *Twenty-second Symposium (International) on Combustion*, 1988, pp. 1479-1494.

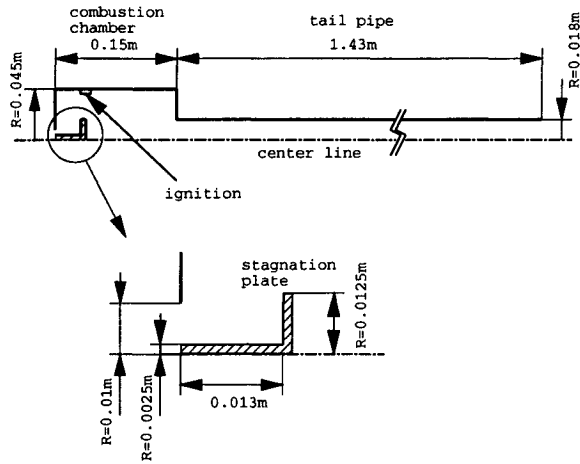


**Fig. 1 Schematic of the pulse combustor.**

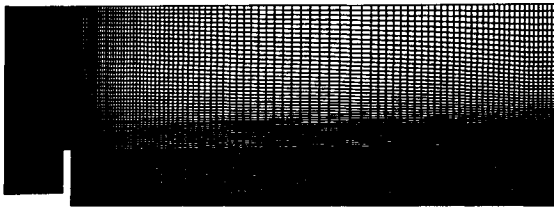


**Fig. 2 Computational grid (focused on around the inlet). Combustion chamber:  $190 \times 80$ , Tail pipe:  $353 \times 48$**

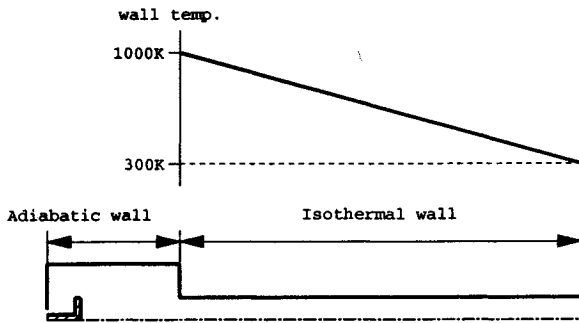


**Fig. 3 Temperature profile for the tail pipe boundary condition.**

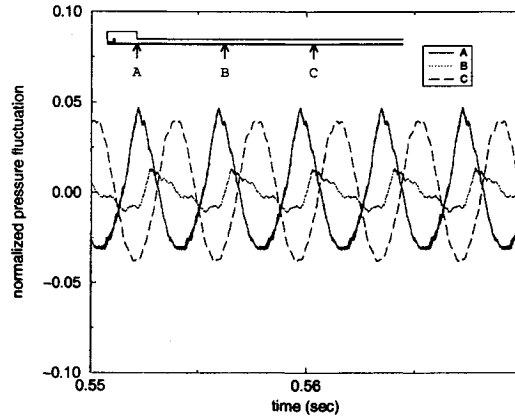


**Fig. 4 Time trace of the oscillating pressure: combustor A, no extinction model.**

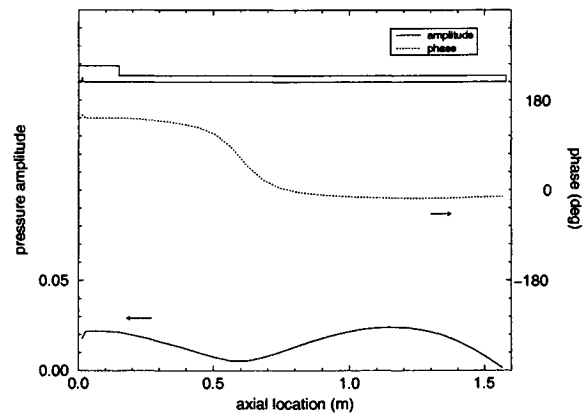


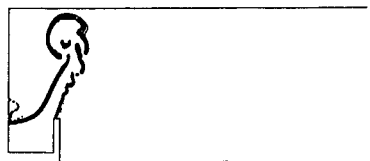
**Fig. 5 Pressure mode shape and phase: combustor A, no extinction model.**



a) cycle time = 0.0



b) cycle time = 0.16



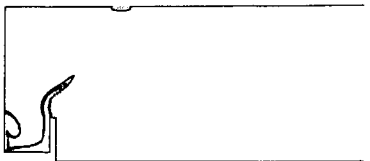
c) cycle time = 0.33



d) cycle time = 0.5



e) cycle time = 0.66

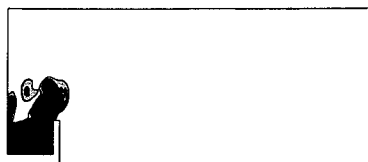


f) cycle time = 0.83

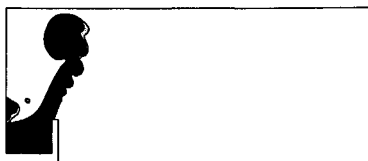
**Fig. 6** Time sequence of the oscillating filtered reaction rate contours ( $\text{kg}/\text{m}^3\text{s}$ ): combustor A, no extinction model.



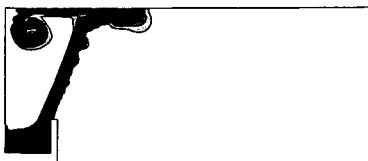
a) cycle time = 0.0



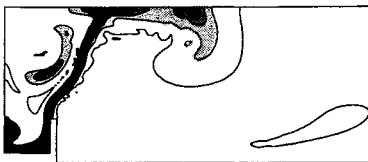
b) cycle time = 0.16



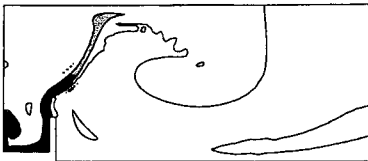
c) cycle time = 0.33



d) cycle time = 0.5

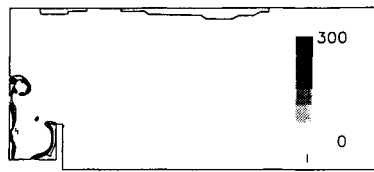


e) cycle time = 0.66

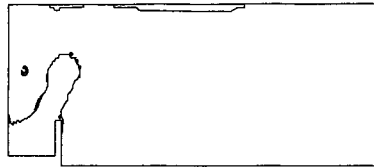


f) cycle time = 0.83

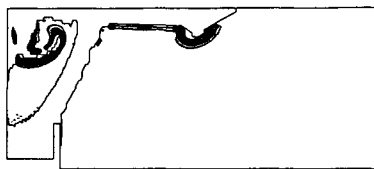
**Fig. 7** Time sequence of the oscillating filtered temperature contours (K): combustor A, no extinction model.



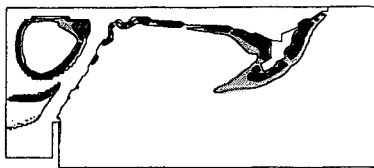
a) cycle time = 0.0



b) cycle time = 0.16



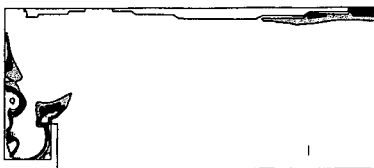
c) cycle time = 0.33



d) cycle time = 0.5

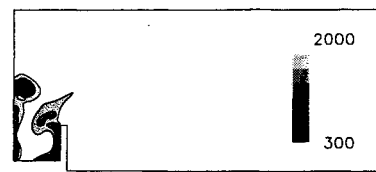


e) cycle time = 0.66

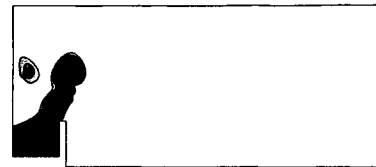


f) cycle time = 0.83

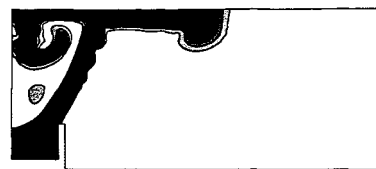
**Fig. 8** Time sequence of the oscillating filtered reaction rate contours ( $\text{kg}/\text{m}^3\text{s}$ ): combustor A, with extinction model.



a) cycle time = 0.0



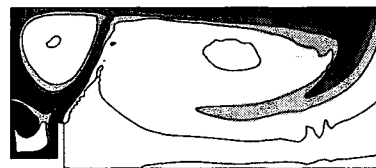
b) cycle time = 0.16



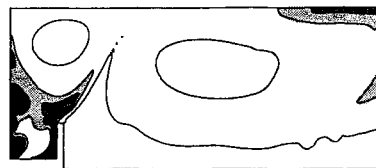
c) cycle time = 0.33



d) cycle time = 0.5



e) cycle time = 0.66



f) cycle time = 0.83

**Fig. 9** Time sequence of the oscillating filtered temperature contours (K): combustor A, with extinction model.

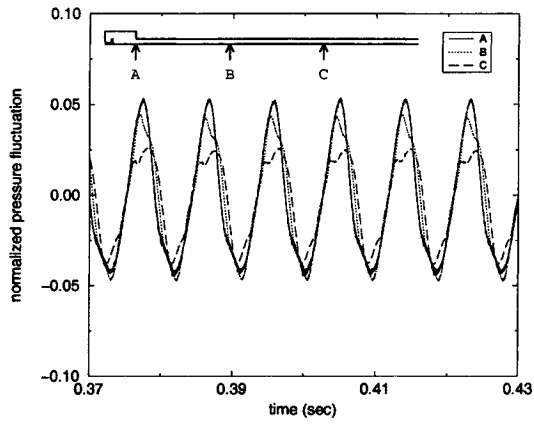
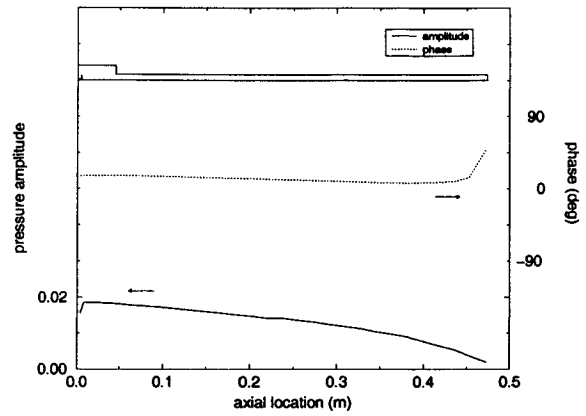


**Fig. 10 Time trace of the oscillating pressure: combustor A, with extinction model.**



**a) combustor B**

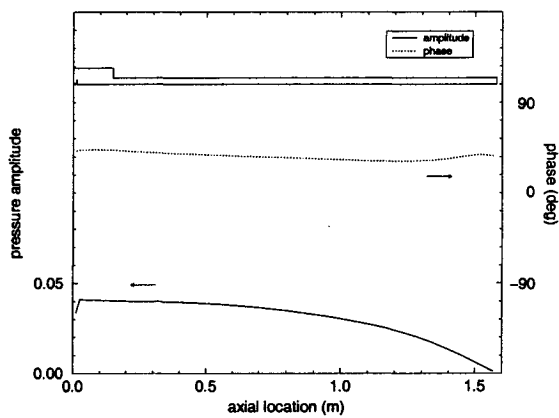
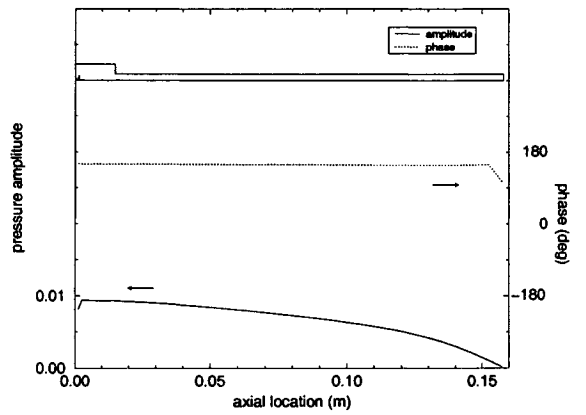
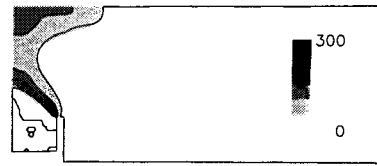


**Fig. 11 Pressure mode shape and phase: combustor A, with extinction model.**

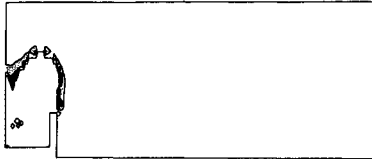


**b) combustor C**

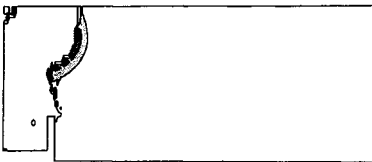
**Fig. 12 Pressure mode shape and phase: combustor B and C, with extinction model.**



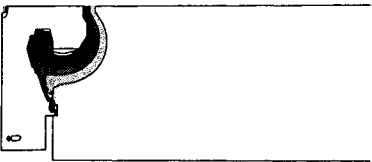
a) cycle time = 0.0



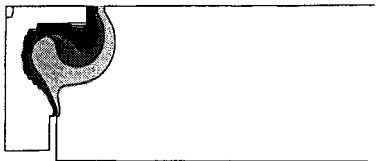
b) cycle time = 0.16



c) cycle time = 0.33



d) cycle time = 0.5

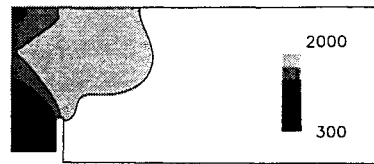


e) cycle time = 0.66

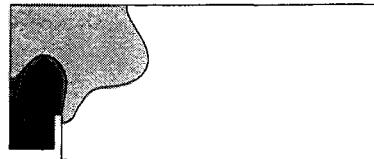


f) cycle time = 0.83

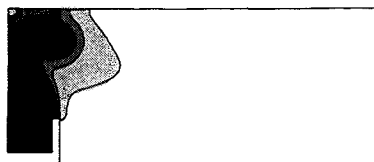
**Fig. 13** Time sequence of the oscillating filtered reaction rate contours ( $\text{kg}/\text{m}^3\text{s}$ ): combustor C, with extinction model.



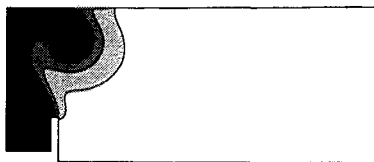
a) cycle time = 0.0



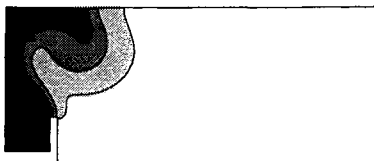
b) cycle time = 0.16



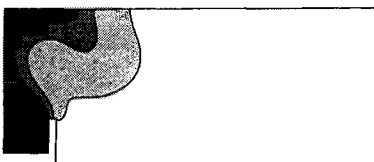
c) cycle time = 0.33



d) cycle time = 0.5



e) cycle time = 0.66



f) cycle time = 0.83

**Fig. 14** Time sequence of the oscillating filtered temperature contours (K): combustor C, with extinction model.